Carbon Monoxide Clathrate Hydrates: Equilibrium Data and Thermodynamic Modeling

Amir H. Mohammadi, Ross Anderson, and Bahman Tohidi
Centre for Gas Hydrate Research, Institute of Petroleum Engineering,
Heriot-Watt University, Edinburgh, EH14 4AS, U.K.

DOI 10.1002/aic.10526
Published online August 19, 2005 in Wiley InterScience (www.interscience.wiley.com).

Carbon monoxide occurs in abundance throughout the cosmos, potentially in clathrate form, whereas on Earth, it forms a notable constituent of industrial flue gases. It has been proposed that hydrate technology could be used in CO_2 separation from flue gases, and in subsea flue gas CO_2 disposal. This—and the likely widespread occurrence of CO clathrates in the cosmos—means it is important that the phase behavior of CO hydrates is known. Here, we present experimental H-L-V (hydrate–liquid–vapor) equilibrium data for CO, CO–CO_2, and CO–C_3H_8 (propane) clathrate hydrates. Data were generated by a reliable step-heating technique validated using measured data for CO_2 and CH_4 hydrates. Data for CO and CO–C_3H_8 clathrates have been used in the optimization of Kihara potential parameters for CO, reported here, facilitating the extension of a thermodynamic model to the prediction of CO hydrate equilibria. Model predictions are validated against independent experimental data for CO–CO_2 (structure I) systems, with good agreement being observed. © 2005 American Institute of Chemical Engineers *AIChE J,* 51: 2825–2833, 2005
Keywords: solid–fluid equilibria, model, equation of state, carbon monoxide, clathrate hydrate, experimental data

Introduction

Gas hydrates, or clathrate hydrates, are a group of nonstoichiometric, icelike crystalline compounds formed through a combination of water and suitably sized "guest " molecules under low-temperature and elevated pressure conditions. In the clathrate lattice, water molecules form hydrogen-bonded cagelike structures, encapsulating the guest molecules, which generally consist of low molecular diameter gases and organic compounds. A concise review of gas hydrates is given by Sloan.[1]

Alongside molecular hydrogen and water, carbon monoxide is one of the most abundant molecules in the cosmos. It is found in solid, gaseous, and potentially clathrate hydrate forms throughout the galaxy, either in interstellar gas clouds, or as a component of comets and planetary bodies.[2-4] In the terrestrial environment, CO forms a notable constituent of flue and other exhaust gases resulting from the combustion of organic materials.

Recently, hydrate technology has been proposed as a means for CO_2 separation from industrial flue gases.[5] Carbon monoxide is a common component of such gases, and thus its effects on hydrate equilibria should be considered in process design. Similarly, any CO present in CO_2 destined for proposed hydrate sequestration schemes[6,7] will also influence the phase behavior. These factors, and the potential widespread abundance of CO clathrates in the cosmos, warrant an improved understanding of CO clathrate hydrate equilibria.

Currently, only very limited data are available in the literature concerning CO hydrates. Carbon monoxide is similar in molecular size to oxygen and nitrogen. Given that both O_2 and N_2 can form simple (single guest) gas hydrates, it was proposed in the 1960s that carbon monoxide should also form clathrates.[2,8,9] In the absence of experimental data, Miller[3] and

Correspondence concerning this article should be addressed to B. Tohidi at bahman.tohidi@pet.hw.ac.uk.

Lunine and Stevenson[4] reached differing conclusions regarding the structure and thermodynamic stability of carbon monoxide hydrates. Miller[3] predicted that CO should form structure II clathrates, with a dissociation pressure of around 13.5 MPa at 273.15 K. Lunine and Stevenson,[4] however, using the classical Lennard–Jones–Devonshire (LJD) cell model (with cell parameters apparently modified from those of nitrogen hydrates), concluded that structure I would be the more stable structure for carbon monoxide, giving a dissociation pressure around 20% lower than that for structure II at the same temperature. Davidson et al.[10] subsequently resolved this issue through low-temperature X-ray powder diffraction studies, which demonstrated that carbon monoxide clathrates have a type I cubic structure with a lattice parameter of 1.188 nm. The authors determined the dissociation pressure of these CO hydrates to be 12.8 MPa at 273.15 K [corresponding to three-phase hydrate–liquid–vapor (*H-L-V*) equilibrium].

Although the results of Davidson et al.[10] provide confirmation that carbon monoxide can form simple clathrate hydrates, to our knowledge no equilibrium data delineating the stability of CO hydrates over a range of temperatures and pressures have been reported. In this work, we present novel carbon monoxide clathrate hydrate dissociation data for the temperature range 274.5 to 284.9 K, at pressures up to 40.3 MPa. Data have also been generated for a carbon monoxide–propane and a carbon monoxide–carbon dioxide gas mixture. Following the procedure suggested by Tohidi-Kalorazi,[11] where Kihara potential parameters are determined through intersection of optimized parameters for structure I and structure II hydrates, measured data for CO–H_2O (structure I forming) and CO–C_3H_8–H_2O (structure II forming) clathrates have been used in the optimization of Kihara potential parameters for CO. Using these optimized Kihara parameters, we have extended an existing thermodynamic model to the prediction of hydrate equilibria involving carbon monoxide. Dissociation data determined for the CO–CO_2–H_2O (structure I hydrate forming) system are used for independent (data not used in model development) model validation, whereas experimental techniques are verified through comparison of measured data for CO_2–H_2O and CH_4–H_2O systems with existing literature data.

Experimental Equipment and Methods

Two different sets of experimental equipment were used to generate the experimental data presented here. These are detailed below.

Setup 1

Setup 1, shown in Figure 1, consists of a 75-cm^3 equilibrium cell (maximum pressure of 41 MPa), removable sample cup, inlet/outlet valve, central PRT (platinum resistance thermometer), Quartzdyne pressure transducer, and a surrounding coolant jacket. The transducer, when used with a personal computer, can measure pressure within a precision of $\pm 6.9 \times 10^{-6}$ MPa and has a quoted accuracy of ± 0.008 MPa for the complete operating range of 0–138 MPa. Cell temperature is controlled by a programmable cryostat (operating temperature range of 253–373 K), and can be kept stable to within ± 0.01 K. Cell temperature and pressure are continuously monitored and recorded by a computer.

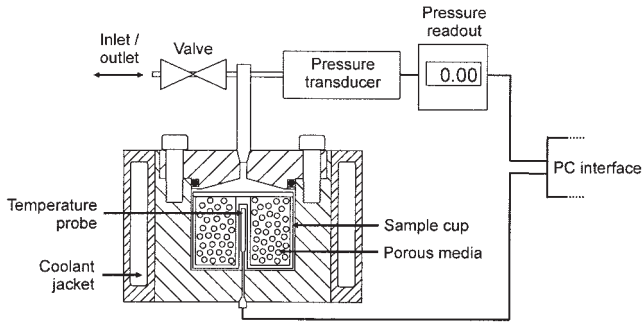

Figure 1. Experimental setup 1.

For sample preparation, the sample cup was first filled with inert silica glass beads of 0.1 mm diameter (to maximize gas–water interfacial area in the absence of mixing), and then placed in the cell. The cell was then evacuated and distilled water injected. After this, the appropriate test gas was added until the desired initial test pressure was achieved.

Setup 2

Setup 2, shown in Figure 2, is composed of a 650-cm^3 cylindrical equilibrium cell (maximum pressure of 69 MPa), surrounding coolant jacket, inlet/outlet valves, PRTs, and Quartzdyne pressure transducer. The transducer can measure pressure within a precision of $\pm 6.9 \times 10^{-6}$ MPa and has a quoted accuracy of ± 0.008 MPa for the complete operating range of 0–138 MPa. Cell temperature is controlled by a programmable cryostat (253–373 K), and can be kept stable to within ± 0.01 K. Cell temperature and pressure are continuously monitored and recorded by a computer. Cell volume, and thus pressure, can be controlled by injection or withdrawal of mercury using a high-pressure pump. The cell is mounted on a pivot mechanism that allows a rocking motion around a horizontal axis. Rocking of the cell and consequent movement of mercury within it aid mixing, thus reducing the time required for systems to achieve equilibrium.

Sample preparation was essentially the same as that for setup 1. The cell was first evacuated, and then distilled water was injected. After this, the appropriate test gas was added, followed by a volume of mercury, until the desired initial test pressure was achieved (the mercury additionally aids mixing).

Dissociation point measurement technique

Incipient *H-L-V* equilibrium conditions were determined by an isochoric step-heating technique following the method of Tohidi et al.[12] The cell, once charged with test fluids, was first cooled rapidly until clathrate formation was observed (from a pressure reduction associated with gas consumption). The temperature was then raised incrementally (0.5 to 1.0 K), with sufficient time being given after each temperature step for the system to reach equilibrium (stable pressure), until the point of complete hydrate dissociation was surpassed. Dissociation conditions were then determined isochorically from heating curve data. The method of step-heating ensures equilibrium at each step, and only equilibrium data are used in determining dissociation conditions. This procedure results in reliable and repeatable measurements.[12]

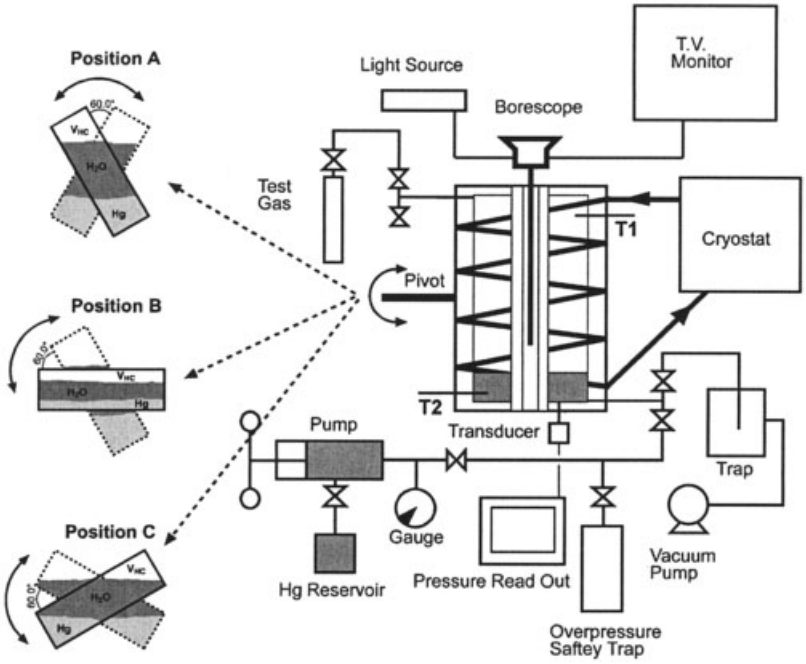

Figure 2. Experimental setup 2.

Position C was used in experiments detailed here.

Experimental Results

Incipient three-phase *H-L-V* equilibrium data have been measured for carbon monoxide, carbon monoxide–carbon dioxide (gas mol fraction: 0.90 CO/0.10 CO_2), and carbon monoxide–propane (gas mol fraction: 0.95 CO/0.05 C_3H_8) clathrate hydrates. For validation of experimental methods, dissociation conditions were additionally determined for CO_2 and CH_4 hydrates. Experimental data are presented in Table 1, and plotted in Figures 3–6. Also shown are thermodynamic predictions, concerning which the reader should refer to the Thermodynamic Modeling section of this work.

Figure 3 shows a comparison of CO_2 and CH_4 hydrate dissociation data determined in this study with data from the literature. The close match observed supports the reliability of experimental methods used in this work.

In Figure 4, measured experimental *H-L-V* data for carbon monoxide clathrate hydrates are compared with literature data for nitrogen hydrates. Lunine and Stevenson,[4] when modeling CO clathrates using the classical LJD cell model, apparently used cell parameters modified from those of nitrogen hydrates (it is assumed because of the similarity in respective molecular diameters). However, data presented in Figure 4 demonstrate

Table 1. Measured (Exp) and Predicted (Pred) *H-L-V* Equilibrium Data for CO–H_2O, CO–CO_2–H_2O, CO–C_3H_8–H_2O, CO_2–H_2O, and CH_4–H_2O Systems*

		T (K)			P			T (K)			P
Setup	Gas	Exp (±0.1)	Pred	AD	(MPa) (±0.007)	Setup	Gas	Exp (±0.1)	Pred	AD	(MPa) (±0.007)
1	CO	274.5	273.8	0.7	13.548	1	0.90 CO	272.9	272.7	0.2	7.203
		276.3	275.9	0.4	16.478		0.10 CO_2	277.0	276.9	0.1	11.663
		278.4	278.1	0.3	20.422			278.8	278.8	0.0	14.613
		279.5	279.4	0.1	23.097			280.9	280.9	0.0	18.866
		281.2	281.1	0.1	27.372	2	0.95 CO	278.2	278.1	0.1	2.579
		282.3	282.4	0.1	30.923		0.05 C_3H_8	283.7	283.6	0.1	5.309
		283.3	283.4	0.1	34.157			286.5	286.0	0.5	7.777
		284.3	284.5	0.2	38.011			292.8	292.0	0.8	19.609
		284.9	285.1	0.2	40.265	2	CH_4	274.6	274.5	0.1	3.060
1	CH_4	280.5	280.3	0.2	5.426			276.2	275.6	0.6	3.446
		283.7	283.5	0.2	7.584			290.6	290.8	0.2	17.257
		285.7	285.7	0.0	9.584			293.6	294.0	0.4	25.841
		286.4	286.4	0.0	10.342			295.8	296.3	0.5	34.584
		289.9	290.1	0.2	15.837			298.3	299.0	0.7	47.863
1	CO_2	277.5	277.4	0.1	2.048						
		282.2	282.3	0.1	3.840						
		282.5	282.6	0.1	4.020						

*Mixed gas compositions given as mole fractions.

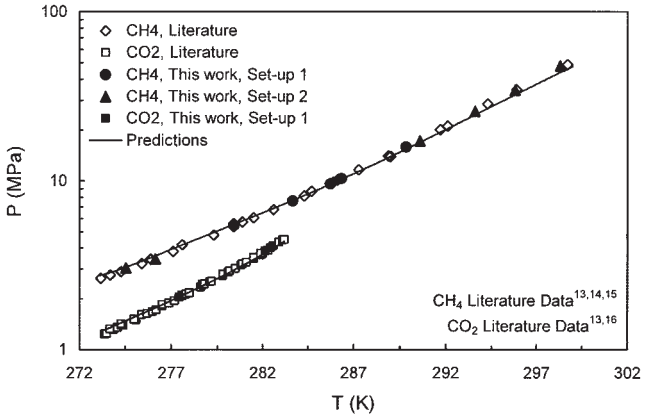

Figure 3. Experimental (this work and literature data) and predicted (this work) *H-L-V* equilibrium data for carbon dioxide and methane hydrates.

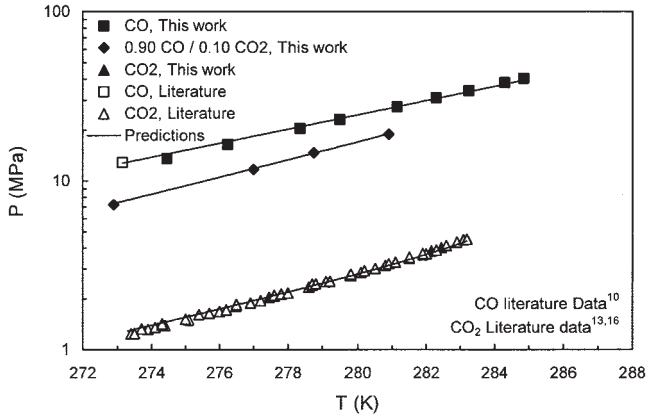

Figure 5. Experimental (this work and literature data) and predicted (this work) *H-L-V* equilibrium data for carbon monoxide, carbon dioxide, and mixed $CO–CO_2$ hydrates (gas composition given as mole fraction).

that CO and N_2 clathrate equilibria are not closely comparable, given that carbon monoxide dissociation conditions are some 2.7 K higher than that for nitrogen hydrates at any given pressure.

Thermodynamic Modeling

A general phase equilibrium model based on the uniformity of component fugacities in all phases[20,21] has been extended to model carbon monoxide clathrate hydrate equilibria. A description of the thermodynamic model is given in Appendix A.

In summary, the statistical thermodynamics model uses the Valderrama modification of the Patel and Teja equation of state[22] (VPT–EoS) and non-density-dependent (NDD) mixing rules[23] for fugacity calculations in all fluid phases. The hydrate phase is modeled using the solid solution theory of van der Waals and Platteeuw,[25] as developed by Parrish and Prausnitz.[26] The equation recommended by Holder et al.[28] is used to calculate the heat capacity difference between the empty hydrate lattice and pure liquid water. The Kihara[29] model for spherical molecules is applied to calculate the potential function for compounds forming hydrate phases. Thermodynamic reference properties for hydrates used in modeling are provided in Table 2.

To extend the thermodynamic model to include CO, the following steps were taken: (1) modeling the phase behavior of pure CO by introducing its physical constants, (2) calculating the water–carbon monoxide binary interaction parameter (BIPs) (using data for aqueous CO solubility), (3) determining binary interaction parameters for CO with other system components, and (4) optimizing Kihara potential parameters for CO.

In this work, carbon monoxide has been added to the thermodynamic model by introducing its physical constants and acentric factor, as reported by Daubert et al.[31] The binary interaction parameter between water and carbon monoxide has been optimized using aqueous carbon monoxide solubility data recommended by Cargill,[32] for the range 273.15–348.15 K and 0.1–1 MPa. A Simplex algorithm was used to optimize the binary interaction parameters. Optimized parameters are pre-

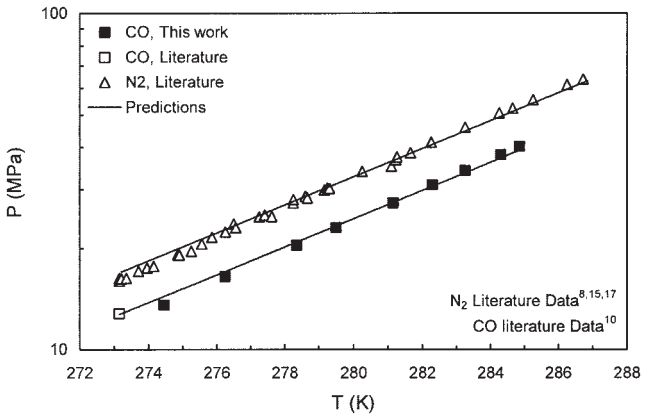

Figure 4. Experimental (this work and literature data) and predicted (this work) *H-L-V* equilibrium data for carbon monoxide and nitrogen hydrates.

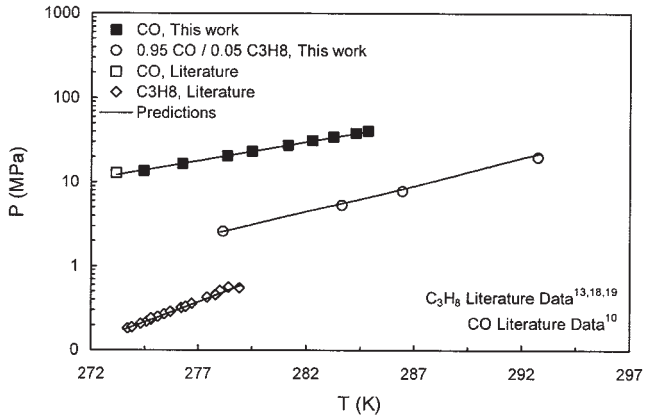

Figure 6. Experimental (this work and literature data) and predicted (this work) *H-L-V* equilibrium data for carbon monoxide, propane, and mixed $CO–C_3H_8$ hydrates (gas composition given as mole fraction).

Table 2. Thermodynamic Reference Properties for Structures I and II Clathrate Hydrates

Parameter	Structure I	Structure II	Data Source
$\Delta\mu_w^0$ (J mol^{-1})	1297	937	Dharmawardhana et al.[30]
Δh_w^0 (J mol^{-1})	1389	1025	Dharmawardhana et al.[30]
Δv_w (cm^3 mol^{-1})	3.0	3.4	Parrish and Prausnitz[26]
ΔC_{Pw}^0 (J mol^{-1} K^{-1})†	−37.32	−37.32	Holder et al.[28]

* In the liquid water region subtract 6009.5 Jmol from Δh_w^0.
**In the liquid water region add 1.601 cm^{3}mol to Δv_w.
† Values to be used in $\Delta C'_{Pw} = \Delta C_{Pw}^0 + 0.179(T - T_0)$.

Table 4. Kihara Potential Parameters for Carbon Monoxide (Newly Reported), Carbon Dioxide, Nitrogen, Methane, and Propane

Hydrate Former	α (Å)	σ^* (Å)*	(ε/k') (K)
CO	0.3976	3.1515	133.61
CO_2**	0.7530	2.9040	171.97
N_2**	0.3350	3.2171	128.39
CH_4**	0.2950	3.2512	153.69
C_3H_8**	0.7300	3.4900	189.27

* $\sigma^* = \sigma - 2\alpha$.
**From Tohidi-Kalorazi.[11]

sented in Table 3. It should be noted that for model predictions presented here, carbon monoxide–carbon dioxide and carbon monoxide–propane binary interaction parameters were set to zero.

The hard-core radius, α, of the Kihara potential parameter for carbon monoxide was calculated to be 0.3976 Å from correlations given by Tee et al.[33] This value was considered acceptable for hydrate modeling, given that predictions are not significantly affected by minor changes in the core radius.[34,35] The two remaining Kihara potential parameters for carbon monoxide—the collision diameter σ and the depth of the energy well ε—were optimized using experimental hydrate dissociation data for carbon monoxide (for structure I) and carbon monoxide–propane systems (for structure II) following the method of Tohidi-Kalorazi[11] (Appendix B). Table 4 presents optimized (for the conditions investigated in this work, using thermodynamic reference properties specified in Table 2) Kihara potential parameters for carbon monoxide, assuming hydrate structure I for simple CO clathrate hydrates.

We have used the resulting model, as detailed above, to predict *H-L-V* equilibria for those systems investigated experimentally. Predictions are compared with experimental data in Figures 3 to 6. Predicted dissociation temperatures and absolute deviations (ADs) from experimental measurements are reported in Table 1. It can be seen that predictions are in good agreement with the experimental data, supporting the reliability of the thermodynamic model. It should be noted that experimental data for carbon monoxide–carbon dioxide clathrate hydrates are independent of the model; only data for pure CO and mixed carbon monoxide–propane hydrates were used to optimize the Kihara potential parameters.

Conclusions

We have reported novel experimental incipient three-phase *H-L-V* equilibrium data for carbon monoxide, carbon monoxide–carbon dioxide, and carbon monoxide–propane clathrate hydrates. Additionally, measured hydrate dissociation data for CO_2 and CH_4 hydrates confirm the reliability of experimental methods used to generate all data. Experimental data for carbon monoxide and carbon monoxide–propane clathrates have been used in the optimization of Kihara potential parameters for carbon monoxide hydrates, reported here, facilitating extension of an existing thermodynamic model to the prediction of clathrate phase equilibria involving CO. Model predictions have been successfully validated against independent experimental equilibrium data for mixed CO–CO_2 (structure I forming) clathrate hydrates.

Acknowledgments

This work was supported by a Scottish Higher Education Funding Council (SHEFC) Research Development Grant, which is gratefully acknowledged. The authors thank Jim Pantling and Colin Flockhart for manufacture and maintenance of experimental equipment.

Notation

AD = absolute deviation: AD = $|T_{Exp} - T_{Pred}|$
BIP = binary interaction parameter
EoS = equation of state
LJD = Lennard-Jones Devonshire
NDD = non-density-dependent mixing rules
N_P = number of data points
VPT–EoS = Valderrama modification of Patel–Teja equation of state
C = Langmuir constant
C' = molar heat capacity
F = parameter of the equation of state
H = hydrate
L = liquid
$\bar{N}$ = an integer equal to 4, 5, 10, or 11
P = pressure
R = gas constant
$\bar{R}$ = cavity radius
T = temperature
V = vapor
$\bar{V}$ = Volume
Z = compressibility factor
Nc = number of components
a = attractive parameter of the equation of state
$\bar{a}$ = parameter of the equation of state
b = parameter of the equation of state
c = parameter of the equation of state
f = fugacity
h = molar enthalpy
k = binary interaction parameter for the classical mixing rules
k' = Boltzmann's constant

Table 3. Gas (1)–Water (2) Binary Interaction Parameters

BIP	CO–H_2O	CO_2–H_2O*	N_2–H_2O*	CH_4–H_2O*	C_3H_8–H_2O*
k_{21}	0.3815	0.1965	0.4792	0.5028	0.5465
l_{21}^1	2.4897	0.7232	2.6575	1.8180	1.6070
$l_{21}^2 \times 10^4$	48.58	23.74	64.46	49.00	39.30

*From Tohidi-Kalorazi.[11]

l = binary interaction parameter for the asymmetric term
n = number of moles
r = distance
v = molar volume
$\bar{v}$ = number of cavities of type m per water molecule in the unit cell
$w(r)$ = spherically symmetric cell potential function
x = mol fraction
z = coordination number

Greek letters

$\Delta C'_{Pw}$ = heat capacity difference between the empty hydrate lattice and liquid water
ΔC^0_{Pw} = reference heat capacity difference between the empty hydrate lattice and liquid water at 273.15 K
Δh_w = enthalpy difference between the empty hydrate lattice and ice/liquid water
Δh^0_w = enthalpy difference between the empty hydrate lattice and ice at ice point and zero pressure
Δv_w = molar volume difference between the empty hydrate lattice and ice/liquid water
$\Delta \mu_w$ = chemical potential difference between the empty hydrate lattice and ice/liquid water
$\Delta \mu^0_w$ = chemical potential difference between the empty hydrate lattice and ice at ice point and zero pressure
$\Delta \mu^{\beta-H}_w$ = chemical potential difference of water between the empty hydrate lattice and the hydrate phase
$\Delta \mu^{\beta-I/L}_w$ = chemical potential difference of water between the empty hydrate lattice and the ice/liquid water phase
Ψ = power parameter in the VPT–EoS
Ω = parameter in the VPT–EoS
α = Kihara hard-core radius
$\alpha(T_r)$ = temperature-dependent function
δ = parameter of cell potential function
ε = characteristic energy
ϕ = fugacity coefficient
μ = chemical potential
σ = collision diameter
σ^* = optimization parameter ($\sigma^* = \sigma - 2\alpha$)
ω = acentric factor
Γ = potential energy of interaction between two molecules

Superscripts

A = asymmetric properties
C = classical properties
H = hydrate
I = ice
L = liquid
sat = property at saturation
β = empty hydrate lattice
0 = reference property
1 = non-temperature-dependent term in NDD mixing rules
2 = temperature-dependent term in NDD mixing rules

Subscripts

I = ice
P = pressure
T = total
Exp = experimental property
Cal = calculated property
Pred = predicted property
a = index for properties
b = index for properties
c = critical property
c^* = index for properties
i, j = molecular species
m = type m of cavities
p = polar compound
r = reduced properties
w = water
0 = reference property
1 = gas
2 = water

Literature Cited

1. Sloan ED. *Clathrate Hydrates of Natural Gases*. 2nd Edition. New York, NY: Marcel Dekker; 1998.
2. Miller SL. The occurrence of gas hydrates in the solar system. *Proc Natl Acad Sci USA*. 1961;47:1798-1808.
3. Miller SL. Clathrate hydrates in the solar system. In: Klinger J, Benest D, Dollfus A, Smoluchowski RJ, eds. *Ices in the Solar System*. Dordrecht, The Netherlands: Kluwer Academic; 1985:59-79.
4. Lunine JI, Stevenson DJ. Thermodynamics of clathrate hydrate at low and high pressures with application to the outer solar system. *Astrophys J Suppl Ser*. 1985;58:493-531.
5. Kang SP, Lee H. Recovery of CO_2 from flue gas using gas hydrate: Thermodynamic verification through phase equilibrium measurements. *Environl Sci Technol*. 2000;34:4397-4400.
6. Sivaraman A. The potential role of hydrate technology in sequestering carbon dioxide. *GasTIPS*. 2003;9:4-7.
7. West OR, Tsouris C, Liang L, Lee SY, McCallum S. Negatively buoyant CO_2 hydrate composite for ocean carbon sequestration. *AIChE J*. 2003;49:283-285.
8. van Cleeff A, Diepen GAM. Gas hydrates of nitrogen and oxygen. *Recl Trav Chim Pays B*. 1960;79:582-586.
9. van Cleeff A, Diepen GAM. Gas hydrates of nitrogen and oxygen. II. *Recl Trav Chim Pays B*. 1965;84:1085-1093.
10. Davidson DW, Desando MA, Gough SR, Handa YP, Ratcliffe CI, Ripmeester JA, Tse JS. A clathrate hydrate of carbon monoxide. *Nature*. 1987;328:418-419.
11. Tohidi-Kalorazi B. *Gas Hydrate Equilibria in the Presence of Electrolyte Solutions*. PhD Thesis. Edinburgh, UK: Heriot-Watt Univ.; 1995.
12. Tohidi B, Burgass RW, Danesh A, Østergaard KK, Todd AC. Improving the accuracy of gas hydrate dissociation point measurements. *Ann NY Acad Sci*. 2000;912:924-931.
13. Deaton WM, Frost EM. Gas hydrates and their relation to the operation of natural gas pipe lines. *US Bur Mines Monogr*. 1946;8:101-108.
14. Mcleod HO, Campbell JM. Natural gas hydrates at pressures to 10,000 psia. *J Petrol Technol*. 1961;222:590-595.
15. Jhaveri J, Robinson DB. Hydrates in the methane–nitrogen system. *Can J Chem Eng*. 1965;43:75-78.
16. Larson SD. *Phase Studies Involving the Two-Component Carbon Dioxide–Water System, Involving the Carbon Dioxide Hydrate*. PhD Thesis. Champaign, IL: Univ. of Illinois; 1955.
17. Marshall DR, Saito S, Kobayashi R. Hydrates at high pressures: Part I. Methane–water, argon–water, and nitrogen–water systems. *AIChE J*. 1964;10:202-205.
18. Verma VK. *Gas Hydrates from Liquid Hydrocarbon–Water Systems*. PhD Thesis. Ann Arbor, MI: Univ. of Michigan; 1974.
19. Robinson DB, Mehta BR. Hydrates in the propane–carbon dioxide–water system. *J Can Petrol Technol*. 1971;10:33-35.
20. Avlonitis DA. *Thermodynamics of Gas Hydrate Equilibria*. PhD Thesis. Edinburgh, UK: Heriot-Watt Univ.; 1992.
21. Tohidi B, Burgass RW, Danesh A, Todd AC. Hydrate inhibition effect of produced water, Part 1. Ethane and propane simple gas hydrates. SPE 26701. Proc of the SPE Offshore Europe 93 Conference; 1993: 255-264.
22. Valderrama JO. A generalized Patel–Teja equation of state for polar and non-polar fluids and their mixtures. *J Chem Eng Jpn*. 1990;23:87-91.
23. Avlonitis D, Danesh A, Todd AC. Prediction of VL and VLL equilibria of mixtures containing petroleum reservoir fluids and methanol with a cubic EoS. *Fluid Phase Equilib*. 1994;94:181-216.
24. Anderson FE, Prausnitz JM. Inhibition of gas hydrates by methanol. *AIChE J*. 1986;32:1321-1333.
25. van der Waals JH, Platteeuw JC. Clathrate solutions. *Adv Chem Phys*. 1959;2:1-57.
26. Parrish WR, Prausnitz JM. Dissociation pressures of gas hydrates formed by gas mixtures. *Ind Eng Chem Process Des Dev*. 1972;11: 26-35.
27. McKoy V, Sinanoğlu O. Theory of dissociation pressures of some gas hydrates. *J Chem Phys*. 1963;38:2946-2956.

28. Holder GD, Corbin G, Papadopoulos KD. Thermodynamic and molecular properties of gas hydrates from mixtures containing methane, argon, and krypton. *Ind Eng Chem Fundam*. 1980;19:282-286.
29. Kihara T. Virial coefficient and models of molecules in gases. *Rev Mod Phys*. 1953;25:831-843.
30. Dharmawardhana PB, Parrish WR, Sloan ED. Experimental thermodynamic parameters for the prediction of natural gas hydrate dissociation conditions. *Ind Eng Chem Fundam*. 1980;19:410-414.
31. Daubert TE, Danner RP, Sibul HM, Stebbins CC. *Physical and Thermodynamic Properties of Pure Chemicals: Data Compilation*. London: Taylor & Francis; 1995.
32. Cargill RW. *IUPAC Solubility Data Series, Vol. 43: Carbon Monoxide*. New York, NY: Pergamon Press; 1990.
33. Tee LS, Gotoh S, Stewart WE. Molecular parameters for normal fluids. *Ind Eng Chem Fundam*. 1966;5:363-367.
34. Holder GD, Hand JH. Multiple-phase equilibria in hydrates from methane, ethane, propane, and water mixtures. *AIChE J*. 1982;28:440-447.
35. Mehta AP, Sloan ED. A thermodynamic model for structure-H hydrates. *AIChE J*. 1994;40:312-320.

Appendix

A. Description of the model

A general phase equilibrium model based on equality of fugacity of each component throughout all the phases[20,21] is used to model the equilibrium conditions. The VPT–EoS[22] with NDD mixing rules[23] are used to determine component fugacities in fluid phases. This equation of state (EoS)[22] is given by

$$P = \frac{RT}{v-b} - \frac{a}{v(v+b)+c(v-b)} \tag{A1}$$

with

$$a = \bar{a}\alpha(T_r) \tag{A2}$$

$$\bar{a} = \frac{\Omega_a R^2 T_c^2}{P_c} \tag{A3}$$

$$b = \frac{\Omega_b R T_c}{P_c} \tag{A4}$$

$$c = \frac{\Omega_{c^*} R T_c}{P_c} \tag{A5}$$

$$\alpha(T_r) = [1 + F(1 - T_r^{\Psi})]^2 \tag{A6}$$

where P, R, and T refer to pressure, gas constant, and temperature, respectively. v, a, $\bar{a}$, b, c, and $\alpha(T_r)$ stand for molar volume, attractive parameter, parameter of the EoS, repulsive parameter, parameter of the EoS, and temperature-dependent function, respectively, and $\Psi = 0.5$. The subscripts c and r denote critical and reduced properties, respectively. The coefficients Ω_a, Ω_b, Ω_{c^*}, and F are given by

$$\Omega_a = 0.66121 - 0.76105 Z_c \tag{A7}$$

$$\Omega_b = 0.02207 + 0.20868 Z_c \tag{A8}$$

$$\Omega_{c^*} = 0.57765 - 1.87080 Z_c \tag{A9}$$

$$F = 0.46283 + 3.58230(\omega Z_c) + 8.19417(\omega Z_c)^2 \tag{A10}$$

where Z_c is the critical compressibility factor and ω is the acentric factor. Tohidi-Kalorazi[11] relaxed the alpha function for water, $\alpha_w(T_r)$, using experimental water vapor pressure data in the range of 258.15 to 374.15 K, to improve the predicted water fugacity:

$$\alpha_w(T_r) = 2.4968 - 3.0661 T_r + 2.7048 T_r^2 - 1.2219 T_r^3 \tag{A11}$$

The above relation is used in the present work.

In this work the NDD mixing rules developed by Avlonitis et al.[23] are applied to describe mixing in the a-parameter

$$a = a^C + a^A \tag{A12}$$

where a^C is given by the classical quadratic mixing rules as follows

$$a^C = \sum_i \sum_j x_i x_j a_{ij} \tag{A13}$$

where x stands for mol fraction and subscripts i and j denote components i and j, respectively. b, c, and a_{ij} parameters are expressed by

$$b = \sum_i x_i b_i \tag{A14}$$

$$c = \sum_i x_i c_i \tag{A15}$$

$$a_{ij} = (1 - k_{ij}) \sqrt{a_i a_j} \tag{A16}$$

where k is the BIP.

The term a^A corrects for asymmetric interaction, which cannot be efficiently accounted for by classical mixing rules

$$a^A = \sum_p x_p^2 \sum_i x_i a_{pi} l_{pi} \tag{A17}$$

$$a_{pi} = \sqrt{a_p a_i} \tag{A18}$$

$$l_{pi} = l_{pi}^1 - l_{pi}^2 (T - T_0) \tag{A19}$$

where p is the index of polar components and l represents the binary interaction parameter for the asymmetric term. Superscripts 1 and 2 refer to non-temperature-dependent and temperature-dependent terms in NDD mixing rules, respectively, and subscript 0 stands for reference property.

Using the VPT–EoS[22] and the NDD mixing rules,[23] the fugacity of each component in all fluid phases is calculated from

$$\ln \phi_i = \frac{1}{RT}\int_{\bar{V}}^{\infty}\left[\left(\frac{\partial P}{\partial n_i}\right)_{T,\bar{V},n_{j\neq i}} - RT/\bar{V}\right]d\bar{V} - \ln Z \quad \text{for } i = 1, 2, \ldots, Nc \tag{A20}$$

$$f_i = x_i \phi_i P \tag{A21}$$

where ϕ, n, Z, and f refer to fugacity coefficient, number of moles, compressibility factor, and fugacity, respectively. $\bar{V}$ and Nc are the total volume and number of components, respectively.

The fugacity of ice is rigorously calculated by correcting the saturation fugacity of water at the same temperature by using the Poynting correction

$$f_w^I = \phi_w^{sat} P_I^{sat} \exp\left[\frac{v_I(P - P_I^{sat})}{RT}\right] \tag{A22}$$

where superscripts I and sat stand for ice and saturation conditions, respectively, and subscripts w and I refer to water and ice, respectively. f_w^I is the fugacity of water in the ice phase, ϕ_w^{sat} is the water fugacity coefficient in the vapor phase at pressure equal to the ice vapor pressure, P_I^{sat} is the ice vapor pressure, and v_I is the ice molar volume, respectively.

The ice molar volume v_I is calculated using the following expression[11]

$$v_I = [19.655 + 0.0022364 \times (T - 273.15)] \times 10^{-6} \tag{A23}$$

where v_I and T are in m^3/gmol and K, respectively. The ice vapor pressure P_I^{sat} is calculated using[11]

$$\log(P_I^{sat}) = -1033/T + 51.06 \times \log(T) - 0.09771 \times T + 7.036 \times 10^{-5} \times T^2 - 98.51 \tag{A24}$$

where T and P_I^{sat} are in K and mmHg, respectively.

The fugacity of water in the hydrate phase f_w^H is given by[24]

$$f_w^H = f_w^{\beta} \exp\left(-\frac{\Delta\mu_w^{\beta-H}}{RT}\right) \tag{A25}$$

where superscripts H and β refer to hydrate and empty hydrate lattice, respectively; and μ stands for chemical potential. f_w^{β} is the fugacity of water in the empty hydrate lattice. $\Delta\mu_w^{\beta-H}$ is the chemical potential difference of water between the empty hydrate lattice μ_w^{β} and the hydrate phase μ_w^H, which is given by the following equation[24-26]

$$\Delta\mu_w^{\beta-H} = \mu_w^{\beta} - \mu_w^H = RT\sum_m \bar{v}_m \ln\left(1 + \sum_j C_{mj} f_j\right) \tag{A26}$$

where $\bar{v}_m$ is the number of cavities of type m per water molecule in the unit cell, f_j is the fugacity of the gas component j, and C_{mj} is the Langmuir constant, which is a function of temperature according to the relation[24-26]

$$C_{mj}(T) = \frac{4\pi}{k'T}\int_0^{\infty} \exp\left[-\frac{w(r)}{k'T}\right] r^2 dr \tag{A27}$$

where k' is Boltzmann's constant and $w(r)$ is the spherically symmetric cell potential in the cavity, with r measured from center and depends on the intermolecular potential function chosen for describing the encaged guest–water interaction. In the present work, the Kihara potential function with a spherical core is used[26]

$$\Gamma(r) = \infty \qquad r \leq 2\alpha$$
$$\Gamma(r) = 4\varepsilon\left[\left(\frac{\sigma^*}{r - 2\alpha}\right)^{12} - \left(\frac{\sigma^*}{r - 2\alpha}\right)^{6}\right] \qquad r > 2\alpha \tag{A28}$$

where $\Gamma(r)$ is the potential energy of interaction between two molecules when the distance between their centers is equal to r. ε is the characteristic energy; α is the radius of the spherical molecular core; and $\sigma^* = \sigma - 2\alpha$, where σ is the collision diameter, that is, the distance where $\Gamma = 0$. The Kihara potential parameters α, σ, and ε are taken from Tohidi-Kalorazi[11] (Table 4). Based on the chosen potential energy function the spherically symmetric cell potential in the cavities (Eq. A27) needs to be derived. McKoy and Sinanoğlu[27] summed up all these guest–water binary interactions inside the cell to yield an overall cell potential[26,27]

$$w(r) = 2z\varepsilon\left[\frac{(\sigma^*)^{12}}{\bar{R}^{11} r}\left(\delta^{10} + \frac{\alpha}{\bar{R}}\delta^{11}\right) - \frac{(\sigma^*)^6}{\bar{R}^5 r}\left(\delta^4 + \frac{\alpha}{\bar{R}}\delta^5\right)\right] \tag{A29}$$

where δ is calculated using the following equation

$$\delta^{\bar{N}} = \frac{1}{\bar{N}}\left[\left(1 - \frac{r}{\bar{R}} - \frac{\alpha}{\bar{R}}\right)^{-\bar{N}} - \left(1 + \frac{r}{\bar{R}} - \frac{\alpha}{\bar{R}}\right)^{-\bar{N}}\right] \tag{A30}$$

where z is the coordination number of the cavity, that is, the number of oxygen molecules at the periphery of each cavity; $\bar{R}$ is the cavity radius; r is the distance of the guest molecule from the cavity center; and $\bar{N}$ is an integer equal to 4, 5, 10, or 11.

The fugacity of water in the empty hydrate lattice f_w^{β}, in Eq. A25, is given by[24]

$$f_w^{\beta} = f_w^{I/L} \exp\left(\frac{\Delta\mu_w^{\beta-I/L}}{RT}\right) \tag{A31}$$

where superscript L stands for liquid, $f_w^{I/L}$ is the fugacity of pure ice or liquid water, and the quantity inside the parentheses is given by the following equation[24,28]

$$\frac{\Delta\mu_w^{\beta-I/L}}{RT} = \frac{\mu_w^{\beta}(T,P)}{RT} - \frac{\mu_w^{I/L}(T,P)}{RT} = \frac{\Delta\mu_w^0}{RT_0} - \int_{T_0}^{T} \frac{\Delta h_w^{\beta-I/L}}{RT^2}\,dT + \int_0^P \frac{\Delta v_w^{\beta-I/L}}{RT}\,dP \quad \text{(A32)}$$

where superscript 0 stands for reference property and h refers to molar enthalpy. μ_w^{β} and $\mu_w^{I/L}$ are the chemical potential of the empty hydrate lattice and of pure water in the ice (I) or the liquid (L) state, respectively. $\Delta\mu_w^0$ is the reference chemical potential difference between water in the empty hydrate lattice and pure water in the ice phase at 273.15 K. $\Delta h_w^{\beta-I/L}$ and $\Delta v_w^{\beta-I/L}$ are the molar enthalpy and molar volume differences between an empty hydrate lattice and ice or liquid water. $\Delta h_w^{\beta-I/L}$ is given by the following equation[24,28]

$$\Delta h_w^{\beta-I/L} = \Delta h_w^0 + \int_{T_0}^{T} \Delta C'_{P_w} dT \quad \text{(A33)}$$

where C' and subscript P refer to molar heat capacity and pressure, respectively. Δh_w^0 is the enthalpy difference between the empty hydrate lattice and ice, at the ice point and zero pressure. The heat capacity difference between the empty hydrate lattice and the pure liquid water phase ΔC_{Pw} is also temperature dependent and the equation recommended by Holder et al.[28] is used

$$\Delta C'_{P_w} = -37.32 + 0.179(T - T_0) \qquad T > T_0 \quad \text{(A34)}$$

where $\Delta C'_{P_w}$ is in J mol^{-1} K^{-1}. Furthermore, the heat capacity difference between hydrate structures and ice is set equal to zero.

B. Optimization of Kihara potential parameters

The following procedure has been used for optimization of the Kihara potential parameters using dissociation pressure data of pure and binary systems[11]:

(1) Experimental dissociation pressure data in the *H-L-V* region is used.

(2) The hard-sphere radius α is fixed to the value obtained using correlations given by Tee et al.[33]

(3) Using an initial guess for ε/k' and σ^*, the hydrate dissociation pressure is calculated at each experimental temperature.

(4) σ^* is changed in 0.01-Å steps and at each step the energy parameter ε/k' is adjusted so as to minimize the following objective function

$$\text{Objective function} = \frac{1}{N_P}\sum_{1}^{N_P}\left|\frac{P_{\text{Cal}} - P_{\text{Exp}}}{P_{\text{Exp}}}\right| \quad \text{(B1)}$$

where N_P is the number of data points and subscripts Cal and Exp refer to calculated and experimental properties, respectively. P_{Cal} is calculated using the model described earlier and P_{Exp} is measured experimentally. To be able to compare the deviations in different sources of data, the objective function is divided by N_P. In the process of optimization, ε/k' is changed stepwise ($\Delta\varepsilon/k'$) and the objective function is calculated and compared with the previous one. If the objective function is higher, the value of the step ($\Delta\varepsilon/k'$) is halved, when $\Delta\varepsilon/k' < 10^{-6}$, the ε/k' and objective function are recorded, before changing σ^*.

This method gives the value of ε/k' as a function of σ^*, with a value of the objective function for each pair of the Kihara potential parameters.

In the optimization of the Kihara potential parameters, the objective is to improve the predictions for multicomponent systems while keeping the accuracy for pure compounds. This is mainly because the experimental data on pure compounds are supposed to be more accurate and the behavior of these systems are in better agreement with the assumption used for the development of the theory, as proposed by van der Waals and Platteeuw.[25] Therefore,

(5) The ε/k' vs. σ^* curve for the pure system, which has structure I, is plotted as well as the objective function vs. σ^* plot, which could show the range of acceptable pairs of parameters.

(6) Steps 1–5 are repeated for the same compound in another hydrate structure, which has structure II, using binary dissociation pressure data. The objective function vs. σ^* plot will again give an indication of the error.

(7) The intersection of the two ε/k' vs. σ^* plots determines the optimized set of the Kihara potential parameters.

Manuscript received Aug. 9, 2004, and revision received Feb. 12, 2005.